Design of Sliding Mode Techniques for a CMG-based Testbed Attitude Control System

Available online at www.sciencedirect.com

ScienceDirect

IFAC Papers Online CONFERENCE PAPER ARCHIVE

IFAC PapersOnLine 54-14 (2021) 506–511

Design of Sliding Mode Techniques for a CMG-based Testbed Attitude Control System

A. D'Ortona * **E. Capello** ** **S. Satoh** ***

* *Department of Mechanical and Aerospace Engineering, Politecnico di Torino, Corso Duca degli Abruzzi 24, 10129 Torino, Italy*

** *Department of Mechanical and Aerospace Engineering, Politecnico di Torino, and with Institute of Electronics, Computer and Telecommunication Engineering, National Research Council of Italy (CNR-IEIIT), Torino, Italy*

*** *Graduate School of Engineering, Osaka University, 2-1, Yamadaoka, Suita, Osaka 565-0871, Japan*

Abstract: Precise pointing accuracy and rapid maneuvering are two key features for attitude control missions of small spacecraft. Control moment gyroscopes (CMGs) are applied as ideal actuator for large torque output capability but are usually limited due to the problem of inherent mechanical singularity. This paper proposes a robust attitude control methodology, based on Sliding Mode Control (SMC) techniques, in presence of CMG practical restrictions and disturbances. Two second-order SMC techniques are designed, to guarantee accuracy and limited convergence time. Moreover, attitude control torques are generated by means of four single gimbal CMGs in pyramidal configuration, considering the design of an experimental testbed. The effectiveness of the proposed methodologies are shown in simulations, for different mission scenarios, including singularity points.

Keywords: Variable-structure/sliding-mode control, Spacecraft attitude control, Control moment gyroscopes, Space applications

Small satellites have begun to play an important role in the space researches, especially in the study of rapidly attitude change with high slew rate. Precise pointing accuracy and rapid maneuvering are two key features for attitude control missions of small spacecraft. To perform the desired mission, a control moment gyro (CMG) is proposed as actuation system, since it can provide rapid slew capability and high pointing accuracy without consuming propellant. A minimum of three CMGs are employed for proper three axis control of a spacecraft and, for redundancy, pyramid configurations of CMGs are used. However, one severe difficulty that prevents their wide application is their inherent geometric singularity problem. Various efforts have been made to overcome this troublesome problem, and many CMG singularity avoidance methods have been developed, with different advantages and disadvantages (Wie, 2005; Lee et al., 2007; Chakravorty, 2012). Recent researches mainly focus on the application of various modern robust controllers to the attitude tracking problem. Several papers are focusing on the design of Sliding Mode Control (SMC) in which CMGs are used as actuation system. The authors of (Durga Nair et al., 2018) propose a quaternion based robust sliding mode attitude controller for a spacecraft with Single Gimbal Control Moment Gyros (SGCMGs), in presence of uncertainties. Although the authors deeply explained the advantages of using this robust control technique for attitude tracking and regulation, a first-order SMC is adopted in the controller design. In recent years, higher order sliding mode controls (HOSMCs) are mainly considered, which are more useful in handling the chattering effect against external disturbances and unknown friction effects. In (Hao and Matunaga, 2014; Hao et al., 2015; Hao and Matunaga, 2016), HOSMCs are applied on the attitude control system of nano-satellite TSUBAME, developed at University of Tokyo. (Hao and Matunaga, 2014) designed an HOSMC in which uncertainties on the parameters are also included. Moreover, a modified steering logic based on two-norm and least-squares minimization method is introduced for solving the singularity problem of CMGs. (Hao et al., 2015) is proposing the same combination of SMC and steering law, but is showing the real-time implementability of the SMC scheme on hardware in the loop simulations. In (Hao and Matunaga, 2016) an SMC control system is designed for the attitude control, using Rodrigues parametrization, and showing the effectiveness of the implementation by simulations. In a similar way, in (Jia and Xu, 2016), starting from Rodrigues parametrization of the attitude, a decentralized adaptive SMC is designed, including an application to a space manipulator.

In our paper, the main idea is to directly control the nonlinear model, even if a steering law is considered. Second-order SMC-based attitude control systems for the CMG system are designed and the attitude control prob-

[1] This work was partially supported by JSPS KAKENHI Grant Number 20H02171.

10.1016/j.ifacol.2021.10.405

lem is studied considering an experimental testbed with four CMGs in pyramidal configuration. Two sliding mode techniques are designed, in which disturbances due to external torques are considered. Disturbances are strongly affecting the performance of the attitude control systems (Utkin et al., 1999). Particularly, the testbed focused in this paper is affected by gravity torque. An adaptive continuous twisting (Moreno et al., 2015; Edwards and Shtessel, 2016) is introduced, to include gain adaptation in function of the magnitude of external disturbances. The adaptation law is based on the previous work (Mancini and Capello, 2021), in which the controller gains are modulated in function of bounded uncertainties, including limitations of the actuation systems and of on-board hardware. This controller is compared with a super-twisting SMC (STW-SMC), which is widely used in space applications (Shtessel et al., 2014; Capello et al., 2017; Torres et al., 2019; Zhao et al., 2020), since it provides a continuous control law, which steers to zero in finite time both the sliding output and its first time derivative, in the presence of smooth matched disturbances. Two different scenarios are simulated to show the effectiveness of the two control laws.

1. SYSTEM MODEL DEFINITION

In this Section, the attitude dynamics of spacecraft in which CMGs are used as actuation systems is detailed. Moreover, since the present work focuses on the study of a testbed (Higashiyama et al., 2020) (see Fig. 1), which is affected by gravity gradient disturbance, the gravity torque model is also included.

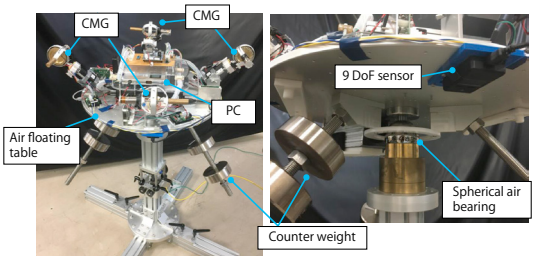

Fig. 1. Testbed with 4 CMGs in pyramidal configuration

1.1 Attitude dynamics and kinematics

The Body Reference Frame (Fig. 2) has been adopted to describe the attitude dynamics once introduced the CMGs to the equations of motion. The origin of the Body Reference Frame is in the CoM of the spacecraft and it is rigidly attached to the body. The Euler's equation can be defined as

$$\mathbf{M}_B = \boldsymbol{\omega}_B \times \mathbf{h}_B + \dot{\mathbf{h}}_B, \tag{1}$$

where $\boldsymbol{\omega_B} \in \mathbb{R}^3$ is the angular velocity, $\mathbf{h}_B \in \mathbb{R}^3$ is the total angular momentum, $\mathbf{M}_B = \mathbf{M}_G + u \in \mathbb{R}^3$ is the total torque applied on the body, $\mathbf{M}_G \in \mathbb{R}^3$ is due to the external disturbances and $u \in \mathbb{R}^3$ is assigned by a control system. The subscript $(\cdot)_B$ indicates that the quantities are written in the Body Reference Frame. The total angular momentum can be split into two terms (Srinivasan et al., 2014), as follows

$$\mathbf{h}_B = \mathbf{h}_B^C + \mathbf{J}_B\boldsymbol{\omega}_B. \tag{2}$$

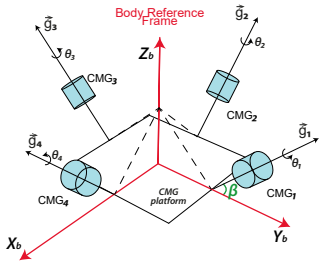

Fig. 2. Configuration of a pyramidal testbed equipped with 4 CMGs

The first term $\mathbf{h}_B^C \in \mathbb{R}^3$ refers only to the CMG system, while the second one $\mathbf{J}_B\boldsymbol{\omega}_B$ is the angular momentum of the spacecraft without considering CMGs, with $\mathbf{J}_B \in \mathbb{R}^{3\times3}$ tensor of inertia matrix. The angular momentum related to the CMG system $\mathbf{h}_B^C$ can be written as function of the angular momentum of each wheel and of the gimbal angle

$$\mathbf{h}_B^C = h_\omega \sum_{i=1}^{4} \mathbf{h}_i(\theta_i), \tag{3}$$

where $\theta_i \in \mathbb{R}$ is the gimbal angle, for $i = 1, ..., 4$, and $h_\omega = \mathrm{J}_\omega\omega_\omega \in \mathbb{R}$ denotes the angular momentum of each wheel (constant). The control input $\mathbf{u} \in \mathbb{R}^3$ can be defined as function of the time derivative of $\mathbf{h}_B^C$

$$\mathbf{u} = -\dot{\mathbf{h}}_B^C - \boldsymbol{\omega} \times \mathbf{h}_B^C. \tag{4}$$

For a cluster of four CMGs, the internal momentum vector $\mathbf{h}_B^C$ and $\dot{\mathbf{h}}_B^C$ are function of the gimbal angle θ_i of each wheel, so

$$\dot{\mathbf{h}}_\mathbf{B}^\mathbf{C} = h_\omega \mathbf{A}(\theta)\dot{\boldsymbol{\theta}}, \tag{5}$$

where $\mathbf{A}(\theta) \in \mathbb{R}^{3\times4}$ transforms the four component vectors derived from CMG cluster in body axes. Considering $s\beta = \sin\beta$ and $c\beta = \cos\beta$, we have

$$\mathbf{A}(\theta) = \begin{bmatrix} -c\beta\cos\theta_1 & \sin\theta_2 & c\beta\cos\theta_3 & -\sin\theta_4 \\ -\sin\theta_1 & -c\beta\cos\theta_2 & \sin\theta_3 & c\beta\cos\theta_4 \\ s\beta\cos\theta_1 & s\beta\cos\theta_2 & s\beta\cos\theta_3 & s\beta\cos\theta_4 \end{bmatrix}. \tag{6}$$

So, the desired control torque can be switched into a command for CMGs in order to have an attitude control by tracking $\dot{\boldsymbol{\theta}}$, where $\dot{\boldsymbol{\theta}} \in \mathbb{R}^4$ is the gimbal rate, and is given by

$$\dot{\boldsymbol{\theta}} = \frac{1}{h_\omega}\mathbf{A}^T(\mathbf{A}\mathbf{A}^T)^{-1}(-\mathbf{u} - \boldsymbol{\omega} \times \mathbf{h}_B^C). \tag{7}$$

The matrix $\mathbf{A}(\theta)$ is not square, so a singularity can occurs. A steering law, as in (Ciavola et al., 2019), is introduced

$$\dot{\boldsymbol{\theta}} = \frac{1}{h_\omega}\mathbf{A}^T(\mathbf{A}\mathbf{A}^T + \lambda\boldsymbol{u_3}\boldsymbol{u_3}^T)^{-1}\dot{\mathbf{h}}_B^C, \tag{8}$$

where λ is a positive scalar parameter related to the Singular Direction Avoidance (SDA) steering law and $\boldsymbol{u_3} \in \mathbb{R}^3$ denotes the eigenvector corresponding to the smallest singular value of $\mathbf{A}$. Moreover, in this paper, quaternion representation is used for the definition of the kinematic equationsas

$$\dot{q} = \frac{1}{2}\Sigma(q)\omega \tag{9}$$

with $q = [q_0, q_v^T]^T = [q_0, q_1, q_2, q_3]^T \in \mathbb{R}^4$, where $q_v =$

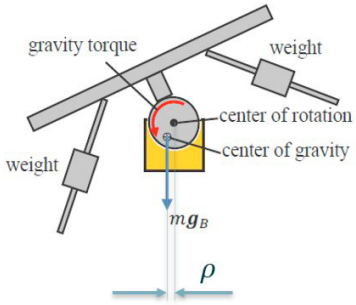

Fig. 3. Gravity torque in the experimental setup (Higashiyama et al., 2020)

$[q_1, q_2, q_3]^T \in \mathbb{R}^3$ is the vectorial part of the quaternion, and q_0 is the scalar one. The matrix $\Sigma(q) \in \mathbb{R}^{4,3}$ is defined as

$$\Sigma(q) = \begin{bmatrix} q_0 & -q_3 & q_2 \\ q_3 & q_0 & -q_1 \\ -q_2 & q_1 & q_0 \\ -q_1 & -q_2 & -q_3 \end{bmatrix}.$$

The quaternion tracking error $\tilde{q}$ is evaluated as

$$\tilde{\mathbf{q}} = \begin{bmatrix} \tilde{q_0} \\ \tilde{\mathbf{q}} \end{bmatrix} = \mathbf{q}^{-1} \otimes \mathbf{q}_r. \tag{10}$$

The subscript $(\cdot)_r$ indicates the desired vector and the symbol $\otimes$ shows the quaternion multiplication. Furthermore, the quaternion inverse is

$$\mathbf{q}^{-1} = [q_0 \ -q_1 \ -q_2 \ -q_3]^T. \tag{11}$$

1.2 Gravity torque disturbance

The main disturbance related to this experimental setup is the torque caused by a misalignment between the center of rotation and the center of gravity of the testbed. In order to minimize this gravity effect, the experimental setup is equipped with three counter weights, which are attached to the testbed by ball screws shown in Fig. 1. The position of the three counter weights has to be adjusted manually, hence it is difficult to obtain a perfect alignment of the center of gravity and of the center of rotation. See Fig. 3 for the scheme of the experimental testbed. During maneuvering, the center of gravity moves, so its position changes with time altering the moment arm. The starting vector which represents the deviation of the center of gravity in the body frame is experimentally estimated as $\boldsymbol{\rho} = [-10, 5, -30]$ μm.

In order to always have the right gravity torque, the vector $\boldsymbol{\rho} \in \mathbb{R}^3$ is multiplied by a rotation matrix $\mathbf{L}_{IB} \in \mathbb{R}^{3\times3}$, so it can be converted in body axes taking into account the rotation of the testbed $\tilde{\boldsymbol{\rho}} = \mathbf{L}_{BI}^{-1}\boldsymbol{\rho}$. The rotation matrix $\mathbf{L}_{IB}$ is a generic transformation matrix, with three rotation angles and 3-2-1 rotation order. From this position vector, the gravity torque is evaluated as $\mathbf{M}_G = m\tilde{\boldsymbol{\rho}} \times \mathbf{g}$, with $\mathbf{g}$ acceleration of gravity. As said before, this disturbance is included in Eq. (1) for the evaluation of the total moment acting on the body.

2. CONTROL SYSTEM DESIGN

Sliding mode is a nonlinear control approach, which is able to ensure high accuracy and excellent robustness against external disturbances and parameter variations with simple design (Levant, 1993; Shtessel et al., 2014). First order SMCs design discontinuous control laws and guarantee the convergence of the sliding surface, denoted by σ, to zero in a finite time (Utkin, 1992). Considering a generic system of states $[x, \dot{x}]$, a first order SMC can be designed as

$$\begin{aligned} \sigma &= cx + \dot{x} \\ u &= -k\text{sgn}(\sigma), \end{aligned} \tag{12}$$

where σ is defined as function of both the state and its time derivative with a constant $c > 0$, u is the control input and $k > m$ is the control parameter, where m denotes a known constant bound of the uncertainty.

In many cases high-frequency switching control is impossible to apply and continuous control is necessary. In the analyzed case, i.e. spacecraft applications, a continuous control input is required due to the actuation system characteristics. For this reason, two second-order SMCs are proposed. Higher order SMCs can steer to zero the sliding output as well as its higher order time derivatives.

2.1 Super-Twisting Sliding Mode Controller

The super-twisting sliding mode control (STW) is a second-order control law and characterized by the following advantages:

- the effect of chattering with STW is reduced compared to classical first-order SMC techniques (Levant, 1993; Shtessel et al., 2014),
- the STW steers to zero both the sliding surface σ and its first time derivative $\dot{\sigma}$ in finite time (Evangelista et al., 2013)
- The controller does not need measurements of $\dot{\sigma}$.

Moreover, the STW-SMC is a continuous controller, which is able to provide all the main SMC properties for systems affected by smooth matched uncertainties/disturbances with bounded gradients. The sliding output for the STW controller is defined as

$$\sigma = \boldsymbol{\omega}_{err} + k_2\tilde{\mathbf{q}}, \tag{13}$$

where $\omega_{err} = \omega_r - \omega$ is the difference between the desired angular velocity ω_r and the current one ω in body axes defined by the Euler equations. k_2 is a positive constant and the quaternion tracking error $\tilde{\mathbf{q}}$ is defined in Eq. (10). One of the control objective is keeping the tracking error on the sliding surface $\sigma = 0$. So, the sliding surface must be *invariant* and its time derivative has to be null. The control input is defined as

$$\begin{aligned} \mathbf{u}_s &= -\lambda|\sigma|^{\frac{1}{2}}\text{sgn}(\sigma) + \mathbf{w} \\ \dot{\mathbf{w}} &= = -\alpha\text{sgn}(\sigma), \end{aligned} \tag{14}$$

where σ is the sliding variable in (13) and the control parameters are chosen such that $\lambda > 1.5L^{\frac{1}{2}}$, $\alpha > 1.1L$, with $L > 0$ known constant bound of the uncertainties (Levant, 1993). According to (Utkin et al., 1999), the performance of sliding mode controllers can be improved including the equivalent control $\mathbf{u}_{eq} \in \mathbb{R}^3$ in the control law definition. It consists in a relation between the control input $\mathbf{u}_s \in \mathbb{R}^3$ and the system dynamics when the sliding mode is reached. Thus, including the equivalent control makes the sliding surface to be more attractive. Finally,

we obtain that the control law applied to the system is the sum of two contributions

$$\mathbf{u} = \mathbf{u}_s + \mathbf{u}_{eq}.$$

Starting from the definition of the first time derivative of the sliding surface and substituting $\dot{\omega}$ of Eq. (1),

$$\dot{\boldsymbol{\sigma}} = \dot{\boldsymbol{\omega}}_r - \dot{\boldsymbol{\omega}} + k\dot{\tilde{\mathbf{q}}} =$$
$$\dot{\boldsymbol{\omega}}_r + \mathbf{J}^{-1}\boldsymbol{\omega} \times \mathbf{J}\boldsymbol{\omega} - \mathbf{J}^{-1}\mathbf{u_s} + \frac{k}{2}[\tilde{q}_0\tilde{\boldsymbol{\omega}} + \tilde{\mathbf{q}} \times (\boldsymbol{\omega}_r + \boldsymbol{\omega})] = 0$$

Note that $M_B = \mathbf{u}_s$ in this case, no external disturbances are included. The equivalent control $\mathbf{u}_{eq}$ can be defined as

$$\mathbf{u}_{eq} = \mathbf{J}\left[\dot{\boldsymbol{\omega}}_r + \frac{k}{2}[\tilde{q}_0\tilde{\boldsymbol{\omega}} + \tilde{\mathbf{q}} \times (\boldsymbol{\omega}_r + \boldsymbol{\omega})]\right] + \boldsymbol{\omega} \times \mathbf{J}\boldsymbol{\omega}. \quad (15)$$

2.2 Adaptive continuous-twisting Sliding Mode Controller

Starting from the works (Shtessel et al., 2014; Moreno et al., 2015; Torres-González et al., 2017), the adaptive continuous twisting has the ability to change its gains in real time to track controlled variables, even if system parameters are unknown or if they change over time. This ability increases the robustness of the control system, since it is able to handle disturbances and adjust the gains.
First, the external disturbance is assumed to be *Lipschitz*, so it is differentiable with bounded derivative, $\dot{d}(t) \leq \mu$. Considering the kinematics equation (Eq. (9)) and manipulating Eq. (1), the following equation is obtained

$$\dot{\boldsymbol{\omega}} = \mathbf{J}^{-1}(\mathbf{u}_s - \boldsymbol{\omega} \times \mathbf{J}\boldsymbol{\omega}) + \mathbf{d}(t), \quad (16)$$

where $\mathbf{d}(t) \in \mathbb{R}^3$ is the disturbance and $\mathbf{u}_s \in \mathbb{R}^3$ is designed as in (Mancini and Capello, 2021)

$$\begin{cases} \mathbf{u}_s = -k_1|\tilde{\mathbf{q}}|^{\frac{1}{3}}\text{sgn}(\tilde{\mathbf{q}}) - k_2|\boldsymbol{\omega}_{err}|^{\frac{1}{2}}\text{sgn}(\boldsymbol{\omega}_{err}) + \boldsymbol{\eta} \\ \dot{\boldsymbol{\eta}} = -k_3|\tilde{\mathbf{q}}|\text{sgn}(\tilde{\mathbf{q}}) - k_4|\boldsymbol{\omega}_{err}|\text{sgn}(\boldsymbol{\omega}_{err}) \end{cases}, \quad (17)$$

where $\boldsymbol{\omega}_{err}$ and $\tilde{\mathbf{q}}$ are defined as in the previous case, $k_j > 0$, $j = 1, ..., 4$ are the controller gains. Since in practical cases the Lipschitz disturbances are usually bounded by $\dot{d}(t) \leq \mu^* = L\mu$, control gains can be scaled as follows (Torres-González et al., 2017)

$$k_{p1} = k_1 L^{\frac{2}{3}} \quad k_{p2} = k_2 L^{\frac{1}{2}} \quad k_{p3} = k_3 L \quad k_{p4} = k_4 L \quad (18)$$

Gains k_j can be substituted by k_{pj}. The adaptation mechanism consisting in varying the gain L, as in (Mancini and Capello, 2021),

$$\begin{aligned} &\dot{L}(t) = l, \quad if\ |\mathbf{x}_e(t)| > \epsilon \quad and \quad L(t) < L_{max}, \\ &\dot{L}(t) = 0, \quad if\ |\mathbf{x}_e(t)| \leq \epsilon \quad and \quad t - t_0 < \tau, \\ &\dot{L}(t) = -l, \quad if\ |\mathbf{x}_e(t)| \leq \epsilon \quad and \quad t - t_0 > \tau \\ &\qquad\qquad\qquad\qquad and \quad L(t) > L_{min} \end{aligned} \quad (19)$$

where l is a positive constant, and $\mathbf{x}_e(t) = [\mathbf{q}_e, \boldsymbol{\omega}_e]^T$ is the state error. When the state error exceeds the required tolerance, L grows until $x_e(t)$ returns to be less than ϵ. After that, if the state errors remain less than ϵ for a time equal to τ, L starts to decrease. The value of l must be chosen in order to compensate the growth of disturbances $\dot{d}$, as detailed in (Mancini and Capello, 2021).

As for the previous case, the control law is the sum of two contributions

$$\mathbf{u} = \mathbf{u}_s + \mathbf{u}_{eq},$$

where $\mathbf{u}_s$ is defined in Eq. (17) and $\mathbf{u}_{eq}$ is in Eq. (15).

3. SIMULATION RESULTS

The performance of the proposed control laws are tested in simulations, starting from the characteristics of the testbed of Fig. 1. The testbed simulates a spacecraft using a metal plate equipped with the four CMGs in pyramidal configuration, a PC, two microcomputers, and three sets of counter weights, as detailed in (Higashiyama et al., 2020). The principal testbed physical properties and input constraints are given in the Table 1. Hardware limitations and limited frequency of control laws are included in simulations. The constraints of the testbed are included to simulate the real behavior of the system and test the performance and the computational effort, for on-board implementations.

Table 1. Physical properties of the testbed

Variable	Numerical value	Units
Mass of testbed m	21.2	kg
Inertia matrix J	$\begin{bmatrix} 0.464 & 0 & 0 \\ 0 & 0.534 & 0 \\ 0 & 0 & 0.610 \end{bmatrix}$	kg/m^2
Angular momentum of each wheel h_ω	0.0576	$kg\,m^2/s$
Skew angle β	45	deg
Gimbal speed const. $\dot{\theta}$	1	rad/s
Gimbal acceleration const. $\ddot{\theta}$	2	rad/s^2
$\bar{\omega}$ const. of the testbed	25	deg/s

The simulation time step and the control laws sample time is 25 ms, which is the sample time of the testbed. Fixed-step simulations are performed in Matlab/Simulink, with `ode4` solver. The initial conditions are in terms of angular velocities $\omega_0 = [0, 0, 0]^T$ and in terms of quaternions $\mathbf{q} = [1, 0, 0, 0]^T$. Moreover, null initial gimbal angles are considered. The desired maximum angular velocities are set to $\omega = [7, 3, 1]^T$ deg/s. A trapezoidal reference variation is considered: (1) in the first 5 seconds of simulation the angular velocity vector is increased to reach the maximum desired angular velocities, (2) the maximum values are maintained for 5 seconds, and finally (3) the angular velocities are decreased to reach the null final values. The reference signals for the vectorial part of the quaternion have been suitably calculated from the kinematic equations, Eq. (9). A simulation time of 20 seconds is considered. The performance of both controllers are shown in simulations, where the gravity torque is considered as an external disturbance. Since the adaptive continuous twisting is able to adapt gains in function of the disturbances, better performance can be observed in terms of angular velocities from Figs. 5 and 7. Instead, the disturbance is not affecting the performance of both controllers in terms of quaternion time history as Figs. 4 and 6 indicate. The control inputs, in terms of gimbal rates as in Eq. (7), are shown in Figs. 8 and 9. The gimbal rates applied by the STW SMC is smaller, compared to the ones applied by the ACTW SMC. Indeed, less control authority is required by the STW SMC when a constant value of angular velocity should be maintained (from 5 to 10 seconds and at the end of simulations). The steady-state errors for both quaternion and angular velocities are analyzed. As deeply explained in (Torres-González et al., 2017), considering the controller sample time Δt_{con}, the accuracy of the steady state error

can be evaluated as $O(\Delta t_{con}^3)$ for $\tilde{\boldsymbol{q}}$, and $O(\Delta t_{con}^2)$ for $\boldsymbol{\omega}_{err}$. Since the time histories of the quaternion vector are similar for both controllers, the tracking error is about 10^{-5}, which is lower than $19\Delta T_{con}^3 = 2.97 \cdot 10^{-4}$, as in (Torres-González et al., 2017) and considering $\Delta t_{con} = 25$ ms. Instead, an oscillatory behavior of the steady-state error for the angular velocities is observed in Fig. 10, showing the residual chattering. The use of smoothing techniques may mitigate, or even eliminate the residual chattering. In Fig. 11, the residual chattering is relaxed, though the residual error is greater than in the STW SMC case.

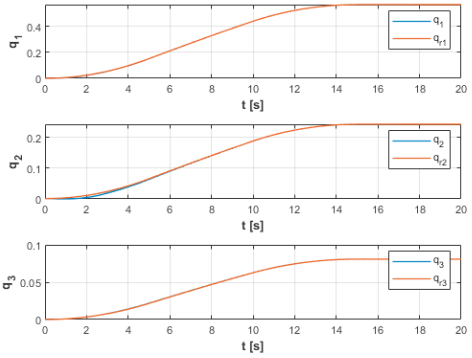

Fig. 4. Vectorial part of the quaternion, when a STW SMCrbance is applied

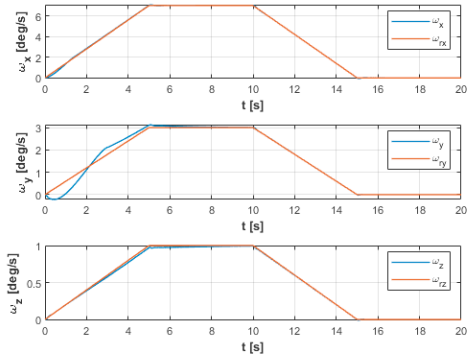

Fig. 5. Variation of the angular velocities, when a STW SMC is applied

4. CONCLUSIONS

In this paper a mathematical model of a CMG-based testbed is developed. A steering law for solving the singularity problem of CMGs and the gravity torque disturbance are introduced. Then, two second order sliding mode strategies are designed to perform the attitude tracking maneuver. Future works will focus on the implementation of the controllers on the testbed and on performing experiments in order to verify the results of simulations. Moreover, to adapt SMC to continuous actuators, some smoothing techniques can be introduced in order to compute a continuous signal by using the hyperbolic tangent or other similar functions, instead of the sgn function.

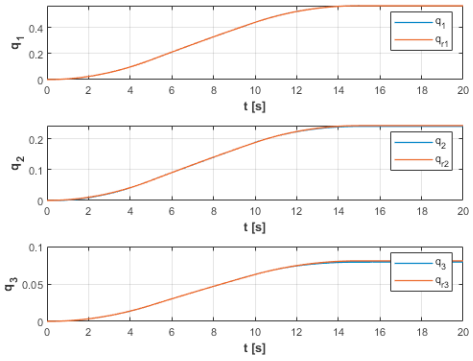

Fig. 6. Vectorial part of the quaternion, when an ACTW SMC is applied

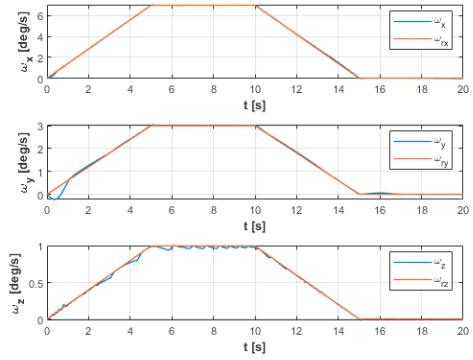

Fig. 7. Variation of the angular velocities, when an ACTW SMC is applied

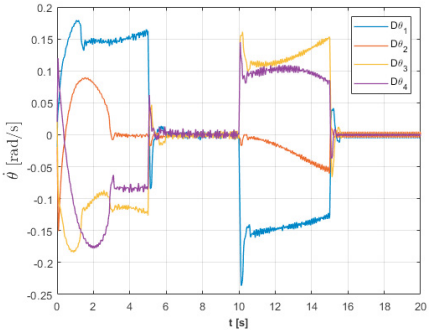

Fig. 8. Time history of gimbal rates, when a STW SMC is applied

REFERENCES

Capello, E., Punta, E., Dabbene, F., Guglieri, G., and Tempo, R. (2017). Sliding-mode control strategies for rendezvous and docking maneuvers. *Journal of Guidance, Control, and Dynamics*, 40(6), 1481–1487.

Chakravorty, J. (2012). Singularity avoidance in single gimbal cmg using the theory of potential functions. In *Proceedings of the 10th World Congress on Intelligent Control and Automation*, 1103–1108.

Ciavola, M., Capello, E., Satoh, S., and Yamada, K. (2019). Comparison of sda and mpc controllers of a cmg system for the singularity problem. In *SICE Annual Conference 2019*.

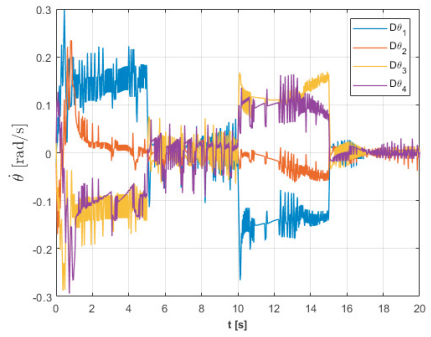

Fig. 9. Time history of gimbal rates, when an ACTW SMC is applied

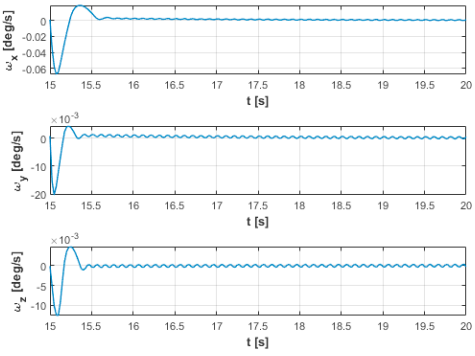

Fig. 10. Angular velocities steady-state error, when a STW SMC and higher disturbance are applied

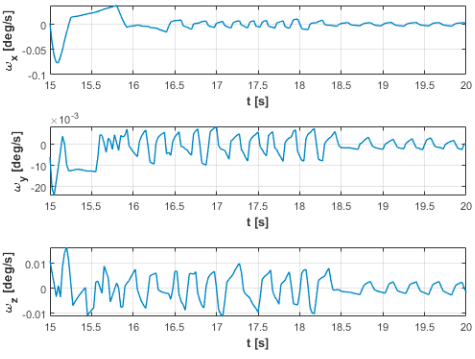

Fig. 11. Angular velocities steady-state error, when an ACTW SMC and higher disturbance are applied

Durga Nair, S., Lal Priya, P.S., and Narayanan, A. (2018). Quaternion based sliding mode attitude controller for a spacecraft with control moment gyros. In *2018 15th International Workshop on Variable Structure Systems (VSS)*, 245–250.

Edwards, C. and Shtessel, Y.B. (2016). Adaptive continuous higher order sliding mode control. *Automatica*, 65, 183–190.

Evangelista, C., Puleston, P., Valenciaga, F., and Fridman, L.M. (2013). Lyapunov-Designed Super-Twisting Sliding Mode Control for Wind Energy Conversion Optimization. *IEEE Transactions on Industrial Electronics*, 60(2), 538–545.

Hao, T., Kawajiri, S., Tawara, K., and Matunaga, S. (2015). A practical rapid attitude maneuver control system using control moment gyros for microsatellite tsubame. *Transactions of the Japan Society for Aeronautical and Space Sciences*, 13, 37–43.

Hao, T. and Matunaga, S. (2014). Robust attitude control of nano-satellite using control moment gyros based on higher order sliding modes. *International Journal of Space Science and Engineering 29*, 2(3), 259–275.

Hao, T. and Matunaga, S. (2016). New sliding mode control approach for rapid attitude maneuver using control moment gyros. *Journal of Aerospace Engineering*, 29(2), 06015001.

Higashiyama, D., Shoji, Y., Satoh, S., Jikuya, I., and Yamada, K. (2020). Attitude control for spacecraft using pyramid-type variable-speed control moment gyros. *Acta Astronautica*, 173, 252–265.

Jia, Y. and Xu, S. (2016). Decentralized adaptive sliding mode control of a space robot actuated by control moment gyroscopes. *Chinese Journal of Aeronautics*, 29(3), 688–703.

Lee, H., Lee, D., Bang, H., and Tahk, M.J. (2007). Singularity avoidance law for cmg using virtual actuator. *IFAC Proceedings Volumes*, 40(7), 305–310.

Levant, A. (1993). Sliding order and sliding accuracy in sliding mode control. *International journal of control*, 58(6), 1247–1263.

Mancini, M. and Capello, E. (2021). Adaptive sliding mode-based control system for flexible spacecraft. In *2021 American Control Conference*.

Moreno, J., Negrete, D., Torres-Gonzlez, V., and Fridman, L. (2015). Adaptive continuous twisting algorithm. *International Journal of Control*, 1–15.

Shtessel, Y., Edwards, C., Fridman, L., and Levant, A. (2014). *Sliding mode control and observation*. Springer Science+Business Media, New York.

Srinivasan, K., Gandhi, D., and Venugopal, M. (2014). Spacecraft attitude control using control moment gyro reconfiguration. *Studies in Informatics and Control*, 23(3), 286.

Torres, J.Z., Cieslak, J., Henry, D., and Dvila, J. (2019). A super-twisting sliding mode control in a backstepping setup for rendezvous with a passive target. *IFAC-PapersOnLine*, 52(12), 25–30.

Torres-González, V., Sanchez, T., Fridman, L.M., and Moreno, J.A. (2017). Design of continuous twisting algorithm. *Automatica*, 80, 119–126.

Utkin, V., Guldner, J., and Shi, J. (1999). Sliding mode control in electromechanical systems. *Taylor & Francis Ltd*, 115–129.

Utkin, V.I. (1992). *Sliding modes in optimization and control problems*. Springer Verlag, New York.

Wie, B. (2005). New singularity escape/avoidance steering logic for control moment gyro systems. *Journal of Guidance Control and Dynamics - J GUID CONTROL DYNAM*, 28, 948–956.

Zhao, Y., Zhang, F., Huang, P., and Liu, X. (2020). Impulsive super-twisting sliding mode control for space debris capturing via tethered space net robot. *IEEE Transactions on Industrial Electronics*, 67(8), 6874–6882.